

Article

Metal Binding Properties of the N-Terminus of the Functional Amyloid Orb2

Thalia H. Bajakian ¹, Silvia A. Cervantes ¹, Maria A. Soria ¹, Maiwenn Beaugrand ^{1,2},
Ji Yun Kim ¹, Rachel J. Service ^{1,3} and Ansgar B. Siemer ^{1,*} 

¹ Department of Biochemistry & Molecular Medicine and the Zilkha Neurogenetic Institute, Keck School of Medicine of USC, Los Angeles, CA 90033, USA; t.bajakian@gmail.com (T.H.B.); angie.crvts@gmail.com (S.A.C.); mariaaco@usc.edu (M.A.S.); maiwenn.beaugrand@gmail.com (M.B.); kim821@usc.edu (J.Y.K.); servicerj@gmail.com (R.J.S.)

² Department of Biomedical Engineering, McGill University, Montreal, QC H3A 2B4, Canada

³ U.S. Army Construction Engineering Research Laboratory, 2902 Newmark Dr, Champaign, IL 61822, USA

* Correspondence: asiemer@usc.edu; Tel.: +1-323-425-2720

Academic Editors: Margaret Sunde, Matthew Chapman and Sarah Perrett

Received: 3 June 2017; Accepted: 21 July 2017; Published: 1 August 2017

Abstract: The cytoplasmic polyadenylation element binding protein (CPEB) homologue Orb2 is a functional amyloid that plays a key regulatory role for long-term memory in *Drosophila*. Orb2 has a glutamine, histidine-rich (Q/H-rich) domain that resembles the Q/H-rich, metal binding domain of the Hpn-like protein (HpnI) found in *Helicobacter pylori*. In the present study, we used chromatography and isothermal titration calorimetry (ITC) to show that the Q/H-rich domain of Orb2 binds Ni²⁺ and other transition metals ions with μ M affinity. Using site directed mutagenesis, we show that several histidine residues are important for binding. In particular, the H61Y mutation, which was previously shown to affect the aggregation of Orb2 in cell culture, completely inhibited metal binding of Orb2. Finally, we used thioflavin T fluorescence and electron microscopy images to show that Ni²⁺ binding induces the aggregating of Orb2 into structures that are distinct from the amyloid fibrils formed in the absence of Ni²⁺. These data suggest that transition metal binding might be important for the function of Orb2 and potentially long-term memory in *Drosophila*.

Keywords: amyloid; protein–metal interaction; aggregation; ITC; thioflavin T fluorescence

1. Introduction

The aggregation of proteins into amyloid fibrils is thought to be a sporadic event in the case of amyloid diseases. However, for functional amyloids, this aggregation is expected to be a tightly regulated process. To understand how the formation of functional amyloid is regulated, we are studying factors that induce and prevent the aggregation of the functional amyloid Orb2 from *Drosophila melanogaster*. Orb2 belongs to the class of cytoplasmic polyadenylation element binding proteins (CPEBs), which are extranuclear regulators of protein expression [1]. CPEBs bind to the cytoplasmic polyadenylation elements in the 3' untranslated region of dormant mRNAs thereby inducing their polyadenylation and translation. In *Aplysia*, the neuronal isoform of CPEB (ApCPEB), which is a key regulator of long-term potentiation (LTP), is activated by undergoing a conformational change from a soluble, oligomeric to an aggregated, amyloid-like state [2,3]. Furthermore, ApCPEB has prion-like properties when introduced into yeast and can form amyloid fibrils in vitro [4,5]. Orb2 is a CPEB homologue in *Drosophila melanogaster* which acts as a key regulator of synapse specific protein expression that is important for maintaining memories beyond 24 h [6–11]. Orb2 has two isoforms, the rare isoform Orb2A and the predominant isoform Orb2B. As shown in Figure 1, Orb2A and Orb2B share the same C-terminus, which is comprised of two RNA recognition motifs (RRMs) and

a zinc finger (Zn). Both isoforms also share a common N-terminal glutamine, histidine rich (Q/H-rich) domain, which is similar to the glutamine, asparagine rich domains that are, e.g., found in yeast prions. However, Orb2A and Orb2B differ at their N-termini as Orb2A only has 21 residues preceding the Q/H-rich domain with residues 1–9 being unique to Orb2A. On the other hand, the N-terminus of Orb2B is 178 residues long.

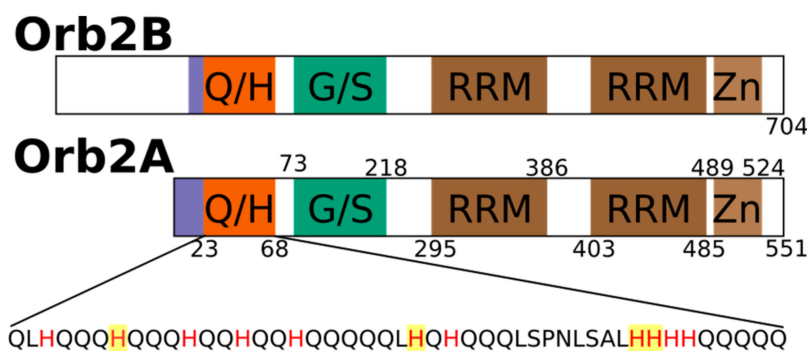


Figure 1. Domain structure of rare isoform Orb2A that is necessary to initiate fibril formation and the predominant isoform Orb2B highlighting the glutamine, histidine rich domain (Q/H), the glycine, serine rich region (G/S), the two RNA recognition motifs (RRM) and the zinc finger (Zn) motif. The sequence of the Q/H-rich domain is shown with all histidines in red and the histidines that were mutated in this study highlighted in yellow.

The N-terminus of Orb2A was found to be important for amyloid formation and long-term memory, as N-terminal deletions prevented long-term memory formation [7] and even point mutations in the N-terminal domain reduced the aggregation propensity of Orb2A in vitro and long-term memory formation in flies [12,13]. We recently found that the N-terminal 21 residues preceding the Q/H-rich domain of Orb2A are sufficient for fibril formation. They form an in-register parallel β -sheet and comprise the static amyloid core of Orb2A1-88 [14]. We also showed that the same N-terminal region of Orb2A can bind to negatively charged lipid vesicles and subsequently form a helical structure that prevents the formation of amyloid fibrils [15]. Surprisingly, the Q/H-rich region of Orb2A1-88 was neither part of the amyloid core nor involved in lipid binding. This poses the following question: what is the role of the Q/H-rich domain of Orb2 if it is not involved in the formation of the amyloid core as originally thought? Interestingly, the Q/H-rich region of Orb2 strikingly resembles the glutamine and histidine rich bacterial Hpn-like protein (HpnI) found in *Helicobacter pylori*, which colonizes the human gut. HpnI has specific Ni^{2+} , Cu^{2+} , Co^{2+} , and Zn^{2+} binding activity that plays a role in nickel storage, which is important for the colonization of the host [16]. Several histidine residues of HpnI were found to be essential for metal binding, while the glutamine residues were responsible for stabilizing the HpnI-metal complex [16,17].

The high histidine content in Orb2's N-terminus and its similarity to HpnI suggests that Orb2 might be able to bind transition metals similar to HpnI. Interestingly, several other amyloid forming proteins, such as amyloid beta ($\text{A}\beta$), α -synuclein, and the prion protein (PrP), have metal binding activity [18]. In the case of $\text{A}\beta$, Cu^{2+} and Zn^{2+} , binding not only modulates aggregation kinetics but was also hypothesized to cause toxicity [19].

In this paper, we ask the following questions: First, does the N-terminal Q/H-rich domain of Orb2 bind transition metals similar to HpnI and other amyloids? Second, which histidine residues are most important for metal binding? Third, what is the effect of the Orb2 metal interaction on the ability of Orb2 to form amyloid fibrils in vitro? In the following, we describe the affinity of Orb2A1-87 (Orb2A87) to several transition metal ions and characterize the effect of metal binding on aggregation kinetics. These results lead to some new hypotheses suggesting that metal interaction might also play

a role in modulating the aggregation kinetics of Orb2 in vivo and could play a role in the regulation of long-term memory in *Drosophila*.

2. Results

2.1. The N-Terminus of Orb2A Binds Transition Metals in the Absence of a Polyhistidine-Tag

To test whether Orb2 binds metals as hypothesized, we cloned the first 88 residues of Orb2A (Orb2A88-His) with a C-terminal polyhistidine-tag and later removed the polyhistidine-tag by mutating in an earlier stop-codon (Orb2A87). Both Orb2A88-His and Orb2A87 bind to nickel charged, nitrilotriacetic acid (Ni-NTA) resin although the binding affinity of Orb2A87 is reduced (data not shown). All experiments described in the following were done on Orb2A87, i.e., without additional polyhistidine-tag. To test whether Orb2A87 binds to metals other than nickel, we tested Orb2A87 binding to NTA resin that was stripped from metal ions and re-charged with Ni²⁺, Cu²⁺, Co²⁺, or Zn²⁺. Soluble recombinant Orb2A87 was bound to these resins at pH 8.0 and eluted from the resin at pH 3.75, at which point the histidine residues are expected to be protonated and lose their metal-binding affinity. As can be seen from Figure 2, Orb2A87 is able to bind to all of these metals ions, but not to the NTA resin without chelated bivalent metal ions. Although the same amount of protein was loaded to the same amount of resin, the intensities of the elution from the Cu-NTA resin is lower, probably because of the lower specificity and higher affinity of this resin [20].

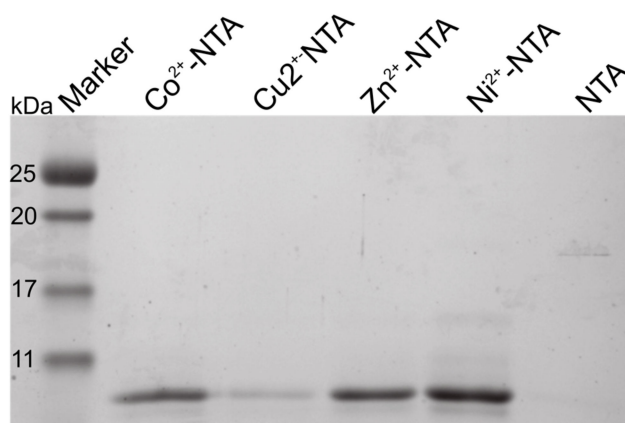


Figure 2. Orb2A87 binds several transition metal ions in the absence of a polyhistidine-tag. Coomassie stained SDS-PAGE showing the purification results of Orb2A87 using nitrilotriacetic acid (NTA) agarose charged with nickel, copper, cobalt, and zinc as well as metal-free NTA agarose. Orb2A87, unlike Orb2A88, has no polyhistidine-tag bound to all of these metals, but did not bind to metal-free NTA agarose.

2.2. Isothermal Titration Calorimetry to Characterize Metal Binding Affinity of Orb2A87

To determine the dissociation constant and number of binding sites of the metal–Orb2A87 complex, we measured isothermal titration calorimetry (ITC) using the following metals ions: Ni²⁺, Cu²⁺, Zn²⁺, Ca²⁺, and Mg²⁺. To slow amyloid formation during these measurements, we measured ITC in the presence of 1 M urea (see Materials and Methods section). Orb2A87 did not have any measurable binding affinity to Ca²⁺ and Mg²⁺. However, we measured μM dissociation constants for Ni²⁺, Cu²⁺, and Zn²⁺ (see Figure 3). The ITC data of both Ni²⁺ and Zn²⁺ fit well to a model of approximately one binding site per monomer. The results of the fits are summarized in Table 1. The binding parameters for Cu²⁺ could not be determined with confidence because it could only be measured in the presence of a weak ligand (glycine), which complicated its analysis [18]. However, the titration curve in Figure 3c indicates that Cu²⁺ has the highest affinity of all metals.

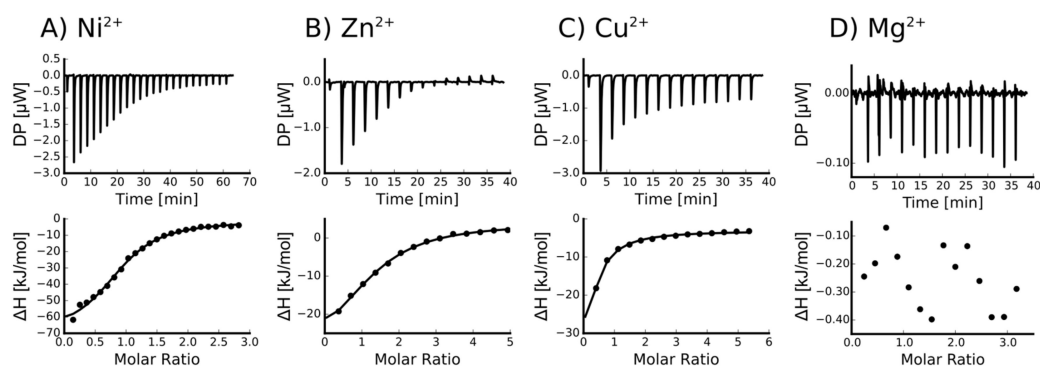


Figure 3. Orb2A87 binds to Ni^{2+} , Zn^{2+} and Cu^{2+} but not to Mg^{2+} . Isothermal titration calorimetry (ITC) titration curves of Orb2A87 with the addition of Ni^{2+} (A); Zn^{2+} (B); Cu^{2+} (C); and Mg^{2+} (D). Both the heat compensation in the sample cell containing Orb2A87 as a function of time (top) and the resulting enthalpy changes as a function of molar addition of metal and the best fit to single binding site model (bottom) are shown.

Table 1. Thermodynamic values for Orb2A87 binding to divalent metal ions as derived from fitting the ITC data shown in Figure 3 to a model assuming a single binding site.

Ligand	<i>n</i> (sites)	K_D (M)	ΔH (kJ/mol)	ΔG (kJ/mol)	$-T\Delta S$ (kJ/mol)
Ni^{2+}	$0.915 \pm 2.2 \cdot 10^{-2}$	$4.66e^{-6} \pm 758 \cdot 10^{-9}$	-69.4 ± 3.57	-31.0	38.4
Zn^{2+}	$1.29 \pm 5.1 \cdot 10^{-2}$	$12.6e^{-6} \pm 2.13 \cdot 10^{-6}$	-37.8 ± 3.53	-28.5	9.38
Cu^{2+}	Not determined *	-	-	-	-
Ca^{2+}	Not binding	-	-	-	-
Mg^{2+}	Not binding	-	-	-	-

* For Cu^{2+} , the binding parameters were not determined since Cu^{2+} binding could only be measured in the presence of a weak binder (Glycine). The number equivalent binding sites is *n*, K_D is the dissociation constant, ΔH the molar heat, ΔG the free energy, and ΔS the entropy of ligand binding.

2.3. Several Histidines Are Important for the Metal Binding Affinity of Orb2A87

To determine the location of the metal binding site of Orb2A87, we introduced several point mutations in the Q/H-rich region, H29A, H46A, H60A, and H61Y. We mutated histidine to tyrosine in the case of H61 because the H61Y mutation was previously shown by Majumdar and co-workers to limit the ability of Orb2A to aggregate in S2 cells [12]. Otherwise, we preferred the more neutral mutation from histidine to alanine. Orb2A87 H29A, H46A, and H60A could still be purified using Ni-NTA affinity chromatography indicating that the metal binding properties of these mutants remained intact. However, H61Y could not be purified this way, indicating that this mutation entirely disrupted the metal affinity of the protein (see Figure 4D). The ITC data shown in Figure 4A–C confirm that H29A, H46A, and H60A still bind nickel. As can be seen from Table 2, the nickel dissociation constants of H29A, H46A, and H60A are still in the μM range, while the number of binding sites (*n*) is decreased to less than 1 per monomer of Orb2A87.

Table 2. Thermodynamic values for Orb2A87 mutants binding to Ni^{2+} derived from fitting the ITC data shown in Figure 4.

Mutant	<i>n</i> (sites)	K_D (M)	ΔH (kJ/mol)	ΔG (kJ/mol)	$-T\Delta S$ (kJ/mol)
H29A	$0.412 \pm 1.1 \cdot 10^{-2}$	$8.21 \cdot 10^{-6} \pm 805 \cdot 10^{-9}$	-61.3 ± 3.48	-29.5	31.7
H46A	$0.715 \pm 6.8 \cdot 10^{-2}$	$4.14 \cdot 10^{-6} \pm 809 \cdot 10^{-9}$	-41.9 ± 6.12	-31.3	10.7
H60A	$0.652 \pm 6.8 \cdot 10^{-2}$	$2.49 \cdot 10^{-6} \pm 1.33 \cdot 10^{-6}$	-41.9 ± 8.06	-32.5	9.41
H61Y	Not binding *	-	-	-	-

* H61Y could not be purified via a Ni-NTA column.

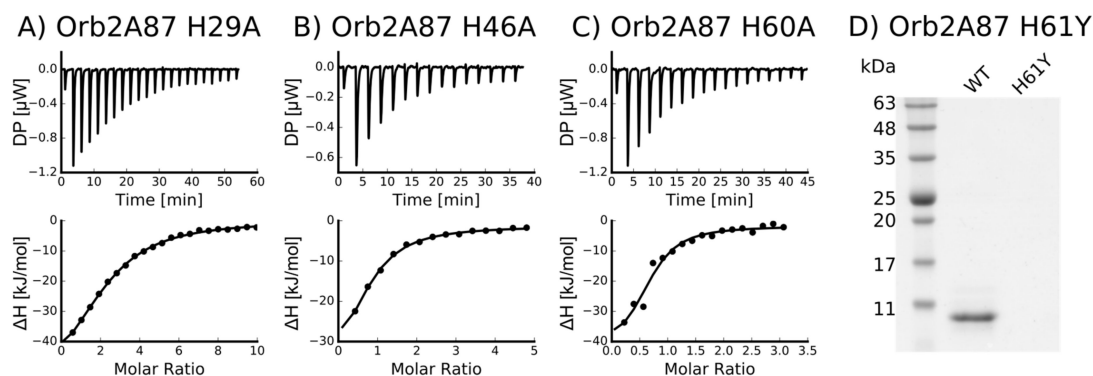


Figure 4. Orb2A87 mutants H29A, H46A and H60A still bind to Ni^{2+} but only with half a binding site per monomer (A–C). ITC Ni^{2+} titration curves of Orb2A87 mutants, H29A (A); H46A (B); H60A (C). Both the heat compensation in the sample cell containing Orb2A87 as a function of time (top) and the resulting enthalpy changes as a function of molar addition of metal and the best fit to single binding site model (bottom) are shown; (D) H61Y does not bind to Ni-NTA resin. SDS-PAGE comparing the Ni-NTA pH 4.25 elution fraction of wild type (WT) Orb2A87 with Orb2A87 H61Y.

2.4. Orb2A–Metal Interaction Affects the Aggregation of Orb2A87

To test the effect of metal binding on the structure of Orb2A87, we recorded circular dichroism (CD) spectra of Orb2A87 in the presence and absence of several metal ions. As can be seen from Figure 5, Orb2A87 has a predominantly random coil conformation in the absence of metal ions as indicated by the minimum at about 202 nm. The addition of the non-binding metals Mg^{2+} and Ca^{2+} did not have any effect on the CD spectrum of Orb2A87. Cu^{2+} , Ni^{2+} , and Zn^{2+} , which bind to Orb2A87, led to a decrease in the CD signal. The overall shape of these less intense spectra stayed the same giving no indication of structural changes. However, the reduction of the CD signal and the absence of an isosbestic point also indicate that part of the sample aggregated and was thus not detected in the presence of Cu^{2+} , Ni^{2+} , and Zn^{2+} .

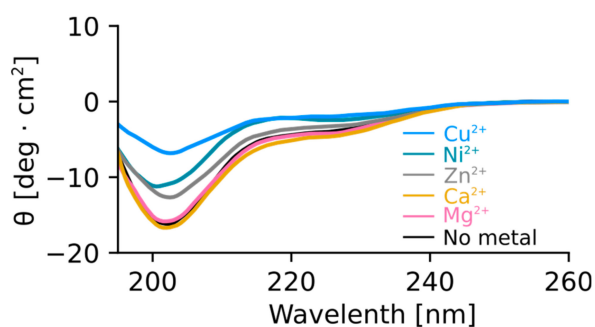


Figure 5. Mg^{2+} and Ca^{2+} do not change the structure of Orb2A87. Cu^{2+} , Ni^{2+} , and Zn^{2+} lead to a decrease in circular dichroism (CD) signal. CD spectra of Orb2A87 without metal and in the presence of 2.5 molar surplus of Cu^{2+} , Ni^{2+} , Zn^{2+} , Ca^{2+} , and Mg^{2+} . The presence of Ca^{2+} and Mg^{2+} does not change the CD spectrum compatible with Orb2A87 in a predominantly random coil conformation. The addition of Cu^{2+} , Ni^{2+} , Zn^{2+} leads to a decay of CD signal with no indication of additional secondary structure.

To study the effect of metal binding on Orb2A87 aggregation and amyloid formation, we measured thioflavin T (ThT) fluorescence kinetics in the absence of metal and in the presence of Ni^{2+} . We used Mg^{2+} , which did not bind to Orb2A87, as a negative control. As can be seen from Figure 6, the addition of Ni^{2+} results in an immediate increase in ThT fluorescence, whereas Orb2A87 alone or in the presence of Mg^{2+} shows an increase in fluorescence after a lag phase of about 3 h. After 10 h, the ThT fluorescence

in the presence of Ni^{2+} starts to decrease again whereas it keeps increasing in the absence of Ni^{2+} . To test whether the immediate increase in ThT fluorescence with the addition of Ni^{2+} was the result of metal induced fibril formation, we took electron microscopy (EM) images from samples that were negatively stained 6 h after the beginning of the aggregation study (i.e., when the ThT fluorescence of the sample containing Ni^{2+} was close to its maximum). As can be seen in Figure 7, both Orb2A87 in the absence of metal or in the presence Mg^{2+} shows the formation of bundled fibrils. However, in the presence of Ni^{2+} , no clear fibrillar structures could be observed and the aggregates looked rather non-specific.

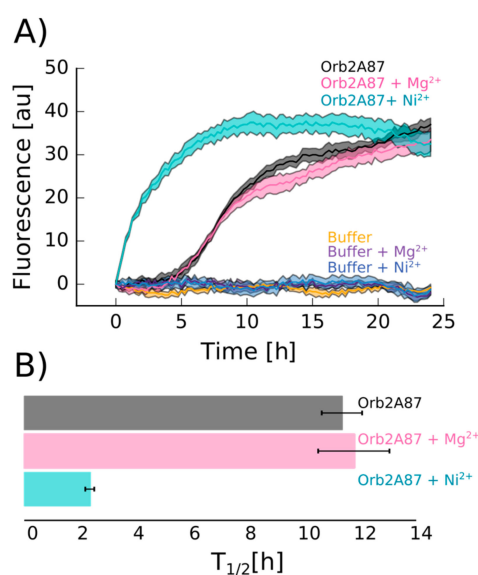


Figure 6. Addition of Ni^{2+} induces rapid increase of thioflavin T (ThT) fluorescence. **(A)** ThT fluorescence kinetics of 17.64 μM Orb2A87 in the absence of metal (black) and in the presence of 2.5 molar excess of Ni^{2+} (cyan) and Mg^{2+} (pink). Buffer control with and without metals shows no fluorescence increase. The average and error of three technical repeats is shown; **(B)** Average of the ThT kinetics half times ($T_{1/2}$) calculated from three independent repeats of the ThT time courses shown in **(A)**.

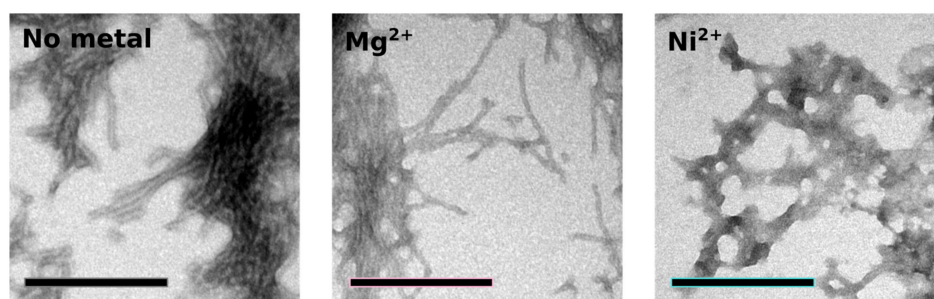


Figure 7. Addition of Ni^{2+} induces aggregation distinct from fibril formation. Electron micrographs of negatively stained aggregates of Orb2A87 collected 6 hours after the start of an aggregation study. Orb2A87 without metal and in the presence of a 2.5 molar excess of Mg^{2+} show typical bundled amyloid fibrils. Aggregates that formed in the presence of a 2.5 molar excess of Ni^{2+} look rather amorphous although high ThT fluorescence was observed in this case. Scale bars: 200 nm.

3. Discussion

The N-Terminus of Orb2A Has an Affinity for Bivalent Metal Ions

In their study of HpnI, Zeng et al. found that HpnI binds bivalent metal ions using ITC. The presence of a similar histidine-rich domain in Orb2 led us to hypothesize that it too possesses

a similar binding affinity for bivalent metal ions. This study confirms this hypothesis using metal affinity chromatography. As shown in Figure 2, Orb2A87 binds to Ni^{2+} , Zn^{2+} , Cu^{2+} , and Co^{2+} chelated to NTA resin. The fact that Orb2A87 did not also elute from the Cu-NTA column, might be a result of its higher binding affinity to this metal [21,22]. Our ITC data in Figure 3 specify that Orb2A87 has one binding site for Ni^{2+} , Zn^{2+} , Cu^{2+} with micromolar affinity. However, Orb2A87 does not bind Mg^{2+} or Ca^{2+} ions, indicating that the metal binding affinity of Orb2 is specific to transition metal ions. Because the Cu^{2+} binding experiment had to be performed in the presence of glycine, a weak ligand, quantitative analysis was not performed, although this interaction seems to have the lowest dissociation constant. Point mutations of several histidine residues in the Q/H-rich region showed that Orb2A87 H61Y abolishes Ni^{2+} binding. In contrast Orb2A87 H29A, H46A, and H60A, still bound Ni^{2+} with micromolar affinity although we observed an apparent decrease in the number of binding sites per Orb2A87 monomer. This reduced number of binding sites suggests that the absence of histidine residues at position 29, 46, and 60 may either reduce the number of monomers capable of binding metal, or require two protein molecules to maintain the metal binding properties of the protein. These observations confirm that the metal binding site of Orb2A87 is indeed located in the Q/H-rich region, specifically in the latter half of the domain, with the H61 residue being necessary for binding. Our CD spectra show that soluble Orb2A87 is mostly disordered in the absence of Ni^{2+} , Zn^{2+} , Cu^{2+} , which is in agreement with our previous CD and Electron Paramagnetic Resonance (EPR) data on the soluble form of Orb2A1-88 [15]. Finally, our CD, ThT, and EM data show that Ni^{2+} binding induces the formation of ThT active Orb2A87 aggregates that are different from the amyloid fibrils observed in the absence of metal. Although an increase in ThT fluorescence has been shown to be relatively specific to amyloid fibrils [23], there are examples of similar increases in fluorescence when ThT binds to monomeric proteins [24] and amorphous aggregates [25]. Although aggregates formed in the presence of Ni^{2+} do not resemble amyloid fibrils, the increase in ThT fluorescence indicates that a ThT binding pocket and possibly a cross β -sheet rich structure is formed upon metal binding.

In summary, our data confirm the original hypothesis that the Q/H rich domain of Orb2 can bind to transition metals via its His residues. Hence, the Q/H rich domain behaves like other H-rich domains, most of which were shown to be metal binding domains. Examples of such domains not only include the Q/H-rich domains of HpnI, but also H-rich domains that are not Q-rich such as the histidine-rich glycoproteins (HRG), Cu and Zn-superoxide dismutase found in *Haemophilus*, and histidine-proline-rich glycoprotein (HPRG) [26–28].

What is the role of the glutamines in Orb2 in the context of metal binding? One possibility is that they help stabilize the metal binding complex similar to Hpn1 [17]. Another possibility is that metal binding induces a structural change, or stabilizes a specific conformation of the glutamines, or both. Finally, metal binding could play a role in stabilizing potential protein–protein interaction of the Q/H-rich domain. Polyglutamine (Poly-Q) domains have been suggested to be involved in coiled-coil protein–protein interfaces [29]. The additional histidines could potentially initiate and strengthen this interaction upon metal binding. For example, ligand interaction of HRGs is enhanced by its interaction with Zn^{2+} [26]. When the Q/H-rich domain of Orb2 is plotted on a helical wheel, the first six histidines fall on the same side, highlighting the potential of a metal stabilized zipper motif for Orb2. Our data clearly show that metal interaction does affect the structure of Orb2A87. However, it will be important to find out in which structural contexts metal binding occurs to determine its exact structural role.

What is the potential function of this metal interaction in long-term memory of *Drosophila*? Majumdar and co-workers showed that the H61Y mutant affected puncta formation of full length Orb2A in S2 cells. They further showed that a different mutation with a similar effect on puncta formation also inhibited long-term memory in flies [12]. Interestingly, H61Y was the only histidine mutation that completely abolished metal binding of Orb2A87. These data suggest that the metal interaction of Orb2 might play a role in its ability to aggregate in cells. Our data show that metal interaction has a pronounced effect on the structure of Orb2A87. We think that the same transition metals will also bind to the Q/H rich domain of full length Orb2A and Orb2B and have a similar

effect on the structure of these proteins. Furthermore, it is possible that in a cellular environment this interaction is crucial for Orb2 aggregation to occur. Since the Q/H rich domain is part of both the rare isoform Orb2A and the predominant isoform OrbB, the effect of metals might be the same for both isoforms and not necessarily be involved in aggregation initiation which requires the unique N-terminus of Orb2A.

If transition metals are an important factor for the function of Orb2, which metal is most likely binding Orb2 in vivo? Several metals have been shown to be important for memory formation. For example, iron and zinc deficiencies affect neuronal development and can lead to memory loss [30–32]. In particular, Zn^{2+} has been associated with memory [33]. It has been shown that Zn^{2+} enters the presynaptic and postsynaptic neurons when released from synaptic vesicles together with glutamate and that this translocation is important for LTP at mossy fibers in rat [34]. Zinc could similarly act as a second messenger on Orb2 during long-term memory formation in *Drosophila* by introducing a structural change or by regulating protein–protein interactions. The basal concentration of free Zn^{2+} in the cytosol is $<10^{-9}$ M, well below the dissociation constant that we determined via ITC. However, during excitation, the intracellular Zn^{2+} concentration can significantly increase [35] potentially inducing structural changes in the Q/H-rich domain of Orb2. The role of these structural changes could be either to initiate the formation of functional Orb2 aggregates, or to induce a non-amyloidogenic, reversible off pathway aggregation that would postpone amyloid formation until the Zn^{2+} concentration goes back to equilibrium.

Further research is necessary to reveal the role of metal binding on the glutamine/histidine rich domain of Orb2 and the effect of this interaction on long-term memory in *Drosophila*.

4. Materials and Methods

4.1. Cloning of Orb2A Mutants

The original pET DEST42 plasmid for Orb2A expression in *Escherichia coli* was provided by Dr. Kausik Si. Starting from this plasmid, we cloned the N-terminal 88 residues of Orb2A into a pET28b vector at the 5' NcoI and 3' XhoI restriction sites. The resulting Orb2A88 Y2G mutation was changed back to the wild type via QuickChange site-directed mutagenesis (Agilent, Santa Clara, CA, USA). The following other mutations were made using QuickChange site-directed mutagenesis: Orb2A87 without polyhistidine-tag (additional stop codon); Orb2A87 H29A; H46A; H60A; H61Y.

The success of cloning and mutagenesis was confirmed via plasmid DNA sequencing.

Primers used (all written from 5' to 3'):

Orb2A88Y2G NcoI GCCCCCTTCACCATGGGCAACAAATTTG
 Orb2A88Y2G XhoI ATAAGCTCGAGCGATCCTCCGCCCTCCTCCACC
 Orb2A88WTsense GAAGGAGATATAACCATGTACAACAAATTTGTTAATTTTCATTTGCGGGTG
 Orb2A88 WT antisense ACCGCAAATGAAATTAACAAATTTGTTGTACATGGTATATCTCCTTC
 Orb2A87 No polyhistidine-tag sense GAGGAGGCGGAGGATAGCTCGAGCACC
 Orb2A87 No polyhistidine-tag antisense GGTGCTCGAGCTATCCTCCGCCCTCCTC
 Orb2A87 H29A sense AGCTCCACCAGCAACAGGCTCAACAACAGCATCAGC
 Orb2A87 H29A antisense GCTGATGCTGTTGTTGAGCCTGTTGCTGGTGGAGCT
 Orb2A87 H46A sense AACAGCAGCAACAGCTCGCTCAGCACCAACAGCAAC
 Orb2A87 H46A antisense GTTGCTGTTGGTGTGAGCGAGCTGTTGCTGCTGTT
 Orb2A87 H60A sense GAATCTGAGTGCCCTGGCCCATCATCACCAGCAG
 Orb2A87 H60A antisense CTGCTGGTGATGATGGGCCAGGGCACTCAGATTC
 Orb2A87 H61Y sense CTGAGTGCCCTGCACTATCATCACCAGCAGC
 Orb2A87 H61Y antisense GCTGCTGGTGATGATAGTGCAGGGCACTCAG

4.2. Protein Expression

E. coli Rosetta 2 (DE3) (Novagen-EMD Millipore, Billerica, MA, USA) was transformed with corresponding pET28b vector. Transformed cells were grown in Luria Bertani (LB) Miller medium with 35 µg/L chloramphenicol and 50 µg/L kanamycin at 30 °C for 15–18 h. Cultures were diluted into LB Miller medium with 35 µg/L chloramphenicol and 50 µg/L kanamycin and grown at 37 °C until the optical cell density at 600 nm reached 0.6. An amount of 1 mM isopropyl 1-thiol-D-galactopyranoside (IPTG) was then added to induce protein expression. Induction proceeded for 16 h while cells remained shaking at 37 °C. Cells were pelleted by centrifugation at 4000× rpm for 20 min using a Sorvall SLC-6000 rotor (Thermo Fisher Scientific Inc., Waltham, MA, USA). Cell pellets were immediately stored at −80 °C.

4.3. Protein Purification

For ITC samples, cells were defrosted on ice and resuspended in denaturing buffer (8 M urea, 10 mM citrate, 100 mM sodium phosphate, 10% glycerol, 0.05% 2-mercaptoethanol) at pH 8.0. The suspended cells were further lysed by sonication for 6 minutes using a cell disruptor sonicator (Heat Systems Model W-220F Qsonica, Newtown, CT, USA). The lysate was later centrifuged at 20,000× rpm for 20 min using a Sorvall ss-34 rotor (Thermo Fisher Scientific Inc.). The resulting supernatant was loaded onto pre-equilibrated Sigma HIS-select Ni-NTA resin (Sigma-Aldrich, St. Louis, MO, USA) and incubated on a shaker at room temperature for at least 1 h. Following incubation, the flow through was collected and the column was washed with denaturing buffer at pH 8.0 to which 0.5% Triton X-100 and 500 mM NaCl were added. The column was subsequently washed with denaturing buffer pH 6.75. Protein was eluted with a pH step gradient in denaturing buffer. The protein predominantly eluted at pH 4.25. The resulting pure protein was either used immediately or frozen in 2 mL aliquots using liquid N₂ and stored at −80 °C.

For samples used in ThT fluorescence and CD assays, protein was purified in the same manner as above. Except for the following modifications: (1) denaturing buffer contained no glycerol and 10 mM Tris instead of citrate; (2) in addition to the Triton X-100, 500 mM NaCl, and pH 6.75 washes, the column was further washed with renaturing buffer (50 mM sodium phosphate, 200 mM NaCl, 10% glycerol, 0.05% 2-mercaptoethanol at pH 8.00) and renaturing buffer containing 20 mM imidazole; (3) the protein was eluted in renaturing buffer containing 250 mM imidazole.

4.4. Affinity Chromatography

To examine Orb2A87 metal affinity, agarose Ni-NTA, Cu-NTA, Co-NTA or Zn-NTA resins were tested individually. Each resin was prepared by regenerating HIS-Select Ni-NTA resin with the desired metal following removal of chelated Ni from the resin according to the protocol listed in the GenScript Technical Manual No. 0237 (Genescript, Piscataway, NJ, USA). HIS-Select Ni-NTA resin was washed with 2 column volumes 6 N GuHCl, 0.2 M Acetic Acid, followed by 5 column volumes of deionized water and 3 column volumes of 2% sodium dodecyl sulfate (SDS). After a wash with 5 column volumes of deionized water, the column was washed with 5 column volumes of 100% ethanol after which the column was washed again with 5 column volumes of deionized water. To remove chelated nickel ions, the column was washed with 5 column volumes of 100 mM ethylenediaminetetraacetic acid (EDTA) pH 8.0 and 5 column volumes of deionized water. To agarose NTA beads, 5 column volumes of a 100 mM stock solution of the desired metal were added (100 mM Co(NO₃)₂·6H₂O, 100 mM CuCl₂·2H₂O, or 100 mM ZnCl₂).

Following equilibration of each column with denaturing buffer, pure Orb2A87 WT was incubated on each metal affinity resin for 1 h. Following incubation, the resin was washed with denaturing buffer pH 8.0. Protein was eluted with denaturing buffer at pH 4.25 to 3.75. Protein elutions were collected and stored at 4 °C, and subsequently analyzed using SDS-PAGE and Coomassie Blue staining.

4.5. ITC Measurements

ITC experiments were performed at 30 °C using a MicroCal PEAQ-ITC microcalorimeter (Malvern Instruments Ltd., Malvern, UK). Orb2A87 samples were prepared using a GE Healthcare PD-10 desalting column (GE Healthcare, Buckinghamshire, UK). Sample was eluted with 1 M urea, 10 mM 4-(2-hydroxyethyl)piperazine-1-ethanesulfonic acid (HEPES), 100 mM NaCl pH 7.4, which was filtered and degassed. Protein concentration was determined using ultraviolet (UV) absorbance at 280 nm and was in the range of 20–50 µM. Metal titrants (0.5–1 mM) were prepared using the same buffer. Fifteen to 25 injections of 2.5 µL metal titrant were titrated into the sample cell over 2.5 s with a stirring speed of 750 × rpm to ensure equilibration. Data were baseline adjusted by subtracting background data obtained from equivalent injections of metal titrant into the buffer solution. The titration curves were analyzed using MicroCal PEAQ-ITC analytics software (version 1.0.0.1259, Malvern Instruments Ltd.) using a model that assumes a set of identical binding sites where the total heat of the solution is calculated as:

$$Q = \frac{nM_t\Delta HV_0}{2} \left(1 + \frac{X_t}{nM_t} + \frac{1}{nKM_t} - \sqrt{\left(1 + \frac{X_t}{nM_t} + \frac{1}{nKM_t} \right)^2 - \frac{4X_t}{nM_t}} \right) \quad (1)$$

where n is the number of binding sites per monomer, M_t is the total concentration of protein, ΔH is the molar heat of ligand binding, X_t the total concentration of ligand, and K the binding constant ($K = 1/K_D$). The heat per injection i can then be calculated via the following equation:

$$\Delta Q(i) = Q(i) + \frac{\Delta V_i}{V_0} \frac{Q(i) + Q(i-1)}{2} - Q(i-1) \quad (2)$$

which compensates for the additional volume (ΔV_i) of each injection. The parameters, n , K , and ΔH are determined using non-linear least square fitting using the Levenberg–Marquardt algorithm.

4.6. Circular Dichroism

Purified Orb2A87 aliquots were buffer exchanged into 75 mM phosphate and 100 mM NaF buffer pH 7.6 using a PD-10 desalting column (GE Healthcare, Chicago, IL, USA). Protein concentration was determined using UV absorbance at 280 nm and calculated to be 19 µM. NiCl₂, MgCl₂, ZnCl₂, CaCl₂, and CuCl₂ were dissolved in deionized H₂O to make 10 mM stock solutions. Metal stocks were added to protein in a 2.5 molar excess of metal over protein, 0.98 µL of each metal stock. For protein with no metals, 0.98 µL deionized H₂O was added. Circular dichroism was measured from 260 nm to 195 nm on a Jasco J-810 spectropolarimeter (Jasco Inc., Easton, MD, USA) at a scan speed of 50 nm/min with data points at every 0.5 nm. Background measurements were taken with buffer and metal or buffer and water to correlate with each sample. Sample and background measurements were averaged over 16 scans. The background spectra were subtracted from each respective sample spectrum and the results were plotted.

4.7. Thioflavin T Fluorescence Assay

The role of metal binding on amyloid formation was tested using the following thioflavin T binding assay. Orb2A87 samples were prepared using GE Healthcare PD-10 desalting columns, and a 20 mM HEPES, 100 mM NaCl pH 7.4 buffer. The eluted samples were pooled and then aliquoted into three fractions of equal volume. Each fraction was aggregated in the presence or absence of the appropriate ligand (Ni²⁺ or Mg²⁺) in a 2.5:1 ligand to protein molar ratio. Samples were measured in triplicate (200 µL fractions plus 2.5 µL of 5 mM thioflavin T stock), using an Eppendorf Plate Reader AF2200 fluorimeter (Eppendorf, Hauppauge, NY, USA). Samples were excited at 440 nm with bandwidth of 20 nm and emission was recorded at 484 nm with a bandwidth of 25 nm. Fluorescence

measurements were taken every 15 min, with 2 s shaking prior to measurement, and over the course of 24 h. Collected data points were averaged and the standard deviation was calculated.

4.8. Electron Microscopy

To observe the morphology of aggregate species used in the thioflavin T binding assay, electron micrographs were prepared for each of the samples described above. A 10 μ L drop of the sample was placed on a sheet of parafilm and a copper mesh electron microscopy grid (Electron Microscopy Sciences, Hatfield, PA, USA) was incubated with the sample for 2 min. Following incubation and removal of excess liquid, 10 μ L of 1% uranyl acetate solution was placed on the grid and incubated for 30 s. Upon removal of excess liquid, the grid was washed with 10 μ L of 1% uranyl acetate and dH₂O, and was dried for 1 h. Grids were imaged using a JEOL JEM-1400 electron microscope (JEOL, Peabody, MA, USA) at 100 kV and photographed using a Gatan digital camera (Gatan Inc., Pleasanton, CA, USA).

Acknowledgments: We would like to acknowledge Kausik Si for providing the expression vector for Orb2A and for fruitful discussion. We would like to acknowledge the USC NanoBiophysics Core and Shuxing Li for his assistance with the Malvern Peaq ITC Microcalorimeter. We would also like to acknowledge Tobias Ulmer, Ralf Langen, Thomas Schmidt, Alan Okada, and Alan Situ for their advice and suggestions. Further, we would like to acknowledge funding from the University of Southern California, the Whitehall Foundation (A.B.S.), the Natural Sciences and Engineering Research Council of Canada (NSERC) Training Program in Bionanomachines and the Canadian Institutes of Health Research Strategic Training Initiative in Chemical Biology (M.B.), and the National Institutes of Health: National Institute of General Medical Sciences (NIGMS) Award R01GM110521 (A.B.S.); National Institute of Neurological Disorders and Stroke (NINDS) Award R01NS084345 (A.B.S., and S.A.C.)

Author Contributions: T.H.B. contributed material, designed and performed experiments, analyzed data, wrote the paper; S.A.C. contributed material, performed experiments, analyzed data; M.A.S. contributed material, performed experiments, analyzed data; J.K. performed experiments; M.B. contributed material; R.J.S. conducted initial studies; A.B.S. conceived and designed the experiments, analyzed data, wrote the paper.

Conflicts of Interest: The authors declare no conflict of interest.

References

1. Ivshina, M.; Lasko, P.; Richter, J.D. Cytoplasmic Polyadenylation Element Binding Proteins in Development, Health, and Disease. *Annu. Rev. Cell Dev. Biol.* **2014**, *30*, 393–415. [[CrossRef](#)] [[PubMed](#)]
2. Si, K.; Choi, Y.-B.; White-Grindley, E.; Majumdar, A.; Kandel, E.R. Aplysia CPEB can form prion-like multimers in sensory neurons that contribute to long-term facilitation. *Cell* **2010**, *140*, 421–435. [[CrossRef](#)] [[PubMed](#)]
3. Si, K.; Giustetto, M.; Etkin, A.; Hsu, R.; Janisiewicz, A.M.; Miniaci, M.C.; Kim, J.-H.; Zhu, H.; Kandel, E.R. A neuronal isoform of CPEB regulates local protein synthesis and stabilizes synapse-specific long-term facilitation in *Aplysia*. *Cell* **2003**, *115*, 893–904. [[CrossRef](#)]
4. Raveendra, B.L.; Siemer, A.B.; Puthanveetil, S.V.; Hendrickson, W.A.; Kandel, E.R.; McDermott, A.E. Characterization of prion-like conformational changes of the neuronal isoform of *Aplysia* CPEB. *Nat. Struct. Mol. Biol.* **2013**, *20*, 495–501. [[CrossRef](#)] [[PubMed](#)]
5. Si, K.; Lindquist, S.; Kandel, E.R. A neuronal isoform of the *Aplysia* CPEB has prion-like properties. *Cell* **2003**, *115*, 879–891. [[CrossRef](#)]
6. Mastushita-Sakai, T.; White-Grindley, E.; Samuelson, J.; Seidel, C.; Si, K. *Drosophila* Orb2 targets genes involved in neuronal growth, synapse formation, and protein turnover. *Proc. Natl. Acad. Sci. USA* **2010**, *107*, 11987–11992. [[CrossRef](#)] [[PubMed](#)]
7. Keleman, K.; Krüttner, S.; Alenius, M.; Dickson, B.J. Function of the *Drosophila* CPEB protein Orb2 in long-term courtship memory. *Nat. Neurosci.* **2007**, *10*, 1587–1593. [[CrossRef](#)] [[PubMed](#)]
8. Stepien, B.K.; Oppitz, C.; Gerlach, D.; Dag, U.; Novatchkova, M.; Krüttner, S.; Stark, A.; Keleman, K. RNA-binding profiles of *Drosophila* CPEB proteins Orb and Orb2. *Proc. Natl. Acad. Sci. USA* **2016**, *113*, E7030–E7038. [[CrossRef](#)] [[PubMed](#)]

9. Krüttner, S.; Stepien, B.; Noordermeer, J.N.; Mommaas, M.A.; Mechtler, K.; Dickson, B.J.; Keleman, K. *Drosophila* CPEB Orb2A Mediates Memory Independent of Its RNA-Binding Domain. *Neuron* **2012**, *76*, 383–395. [[CrossRef](#)] [[PubMed](#)]
10. White-Grindley, E.; Li, L.; Mohammad Khan, R.; Ren, F.; Saraf, A.; Florens, L.; Si, K. Contribution of Orb2A Stability in Regulated Amyloid-Like Oligomerization of *Drosophila* Orb. *PLoS Biol.* **2014**, *12*, e1001786. [[CrossRef](#)] [[PubMed](#)]
11. Khan, M.R.; Li, L.; Pérez-Sánchez, C.; Saraf, A.; Florens, L.; Slaughter, B.D.; Unruh, J.R.; Si, K. Amyloidogenic Oligomerization Transforms *Drosophila* Orb2 from a Translation Repressor to an Activator. *Cell* **2015**, *163*, 1468–1483. [[CrossRef](#)] [[PubMed](#)]
12. Majumdar, A.; Cesario, W.C.; White-Grindley, E.; Jiang, H.; Ren, F.; Khan, M.R.; Li, L.; Choi, E.M.-L.; Kannan, K.; Guo, F.; et al. Critical Role of Amyloid-like Oligomers of *Drosophila* Orb2 in the Persistence of Memory. *Cell* **2012**, *148*, 515–529. [[CrossRef](#)] [[PubMed](#)]
13. Hervás, R.; Li, L.; Majumdar, A.; Fernández-Ramírez, M.C.; Unruh, J.R.; Slaughter, B.D.; Galera-Prat, A.; Santana, E.; Suzuki, M.; Nagai, Y.; et al. Molecular Basis of Orb2 Amyloidogenesis and Blockade of Memory Consolidation. *PLoS Biol.* **2016**, *14*, e1002361. [[CrossRef](#)] [[PubMed](#)]
14. Cervantes, S.A.; Bajakian, T.H.; Soria, M.A.; Falk, A.S.; Service, R.J.; Langen, R.; Siemer, A.B. Identification and Structural Characterization of the N-terminal Amyloid Core of Orb2 isoform A. *Sci. Rep.* **2016**, *6*, 38265. [[CrossRef](#)] [[PubMed](#)]
15. Soria, M.A.; Cervantes, S.A.; Bajakian, T.H.; Siemer, A.B. The functional amyloid Orb2A binds to lipid membranes. *Biophys. J.* **2017**, *113*, 37–47. [[CrossRef](#)] [[PubMed](#)]
16. Zeng, Y.-B.; Yang, N.; Sun, H. Metal-binding properties of an Hpn-like histidine-rich protein. *Chem. Eur. J.* **2011**, *17*, 5852–5860. [[CrossRef](#)] [[PubMed](#)]
17. Chiera, N.M.; Rowinska-Zyrek, M.; Wieczorek, R.; Guerrini, R.; Witkowska, D.; Remelli, M.; Kozłowski, H. Unexpected impact of the number of glutamine residues on metal complex stability. *Metallomics* **2013**, *5*, 214–221. [[CrossRef](#)] [[PubMed](#)]
18. Hong, L.; Simon, J.D. Insights into the thermodynamics of copper association with amyloid- β , α -synuclein and prion proteins. *Metallomics* **2011**, *3*, 262–266. [[CrossRef](#)] [[PubMed](#)]
19. Tõugu, V.; Tiiman, A.; Palumaa, P. Interactions of Zn(II) and Cu(II) ions with Alzheimer’s amyloid- β peptide. Metal ion binding, contribution to fibrillization and toxicity. *Metallomics* **2011**, *3*, 250–261. [[CrossRef](#)] [[PubMed](#)]
20. Volz, J.; Uwe Bosch, F.; Wunderlin, M.; Schuhmacher, M.; Melchers, K.; Bensch, K.; Steinhilber, W.; Schäfer, K.P.; Tóth, G.; Penke, B.; et al. Molecular characterization of metal-binding polypeptide domains by electrospray ionization mass spectrometry and metal chelate affinity chromatography. *J. Chromatogr. A* **1998**, *800*, 29–37. [[CrossRef](#)]
21. Arnold, F.H. Metal-affinity separations: A new dimension in protein processing. *Biotechnology* **1991**, *9*, 151–156. [[CrossRef](#)] [[PubMed](#)]
22. Ueda, E.K.M.; Gout, P.W.; Morganti, L. Current and prospective applications of metal ion-protein binding. *J. Chromatogr. A* **2003**, *988*, 1–23. [[CrossRef](#)]
23. LeVine, H. Thioflavine T interaction with amyloid β -sheet structures. *Amyloid* **1995**, *2*, 1–6. [[CrossRef](#)]
24. Groenning, M.; Olsen, L.; van de Weert, M.; Flink, J.M.; Frokjaer, S.; Jørgensen, F.S. Study on the binding of Thioflavin T to β -sheet-rich and non- β -sheet cavities. *J. Struct. Biol.* **2007**, *158*, 358–369. [[CrossRef](#)] [[PubMed](#)]
25. Ghosh, S.; Pandey, N.K.; Singha Roy, A.; Tripathy, D.R.; Dinda, A.K.; Dasgupta, S. Prolonged Glycation of Hen Egg White Lysozyme Generates Non Amyloid Structures. *PLoS ONE* **2013**, *8*, 1–15. [[CrossRef](#)] [[PubMed](#)]
26. Jones, A.L.; Hulett, M.D.; Parish, C.R. Histidine-rich glycoprotein: A novel adaptor protein in plasma that modulates the immune, vascular and coagulation systems. *Immunol. Cell Biol.* **2005**, *83*, 106–118. [[CrossRef](#)] [[PubMed](#)]
27. Battistoni, A.; Pacello, F.; Mazzetti, A.P.; Capo, C.; Kroll, J.S.; Langford, P.R.; Sansone, A.; Donnarumma, G.; Valenti, P.; Rotilio, G. A histidine-rich metal binding domain at the N terminus of Cu, Zn-superoxide dismutases from pathogenic bacteria. A novel strategy for metal chaperoning. *J. Biol. Chem.* **2001**, *276*, 30315–30325. [[CrossRef](#)] [[PubMed](#)]
28. Ranieri-Raggi, M.; Moir, A.J.G.; Raggi, A. The role of histidine-proline-rich glycoprotein as zinc chaperone for skeletal muscle AMP deaminase. *Biomolecules* **2014**, *4*, 474–497. [[CrossRef](#)] [[PubMed](#)]

29. Schaefer, M.H.; Wanker, E.E.; Andrade-Navarro, M.A. Evolution and function of CAG/polyglutamine repeats in protein-protein interaction networks. *Nucleic Acids Res.* **2012**, *40*, 4273–4287. [[CrossRef](#)] [[PubMed](#)]
30. Fretham, S.; Carlson, E.; Georgieff, M. The role of iron in learning and memory. *Adv. Nutr.* **2011**, *2*, 112–121. [[CrossRef](#)] [[PubMed](#)]
31. Han, M.; Kim, J. Effect of dietary iron loading on recognition memory in growing rats. *PLoS ONE* **2015**, *10*, e0120609. [[CrossRef](#)] [[PubMed](#)]
32. Takeda, A.; Tamano, H. Significance of the degree of synaptic Zn^{2+} signaling in cognition. *BioMetals* **2016**, *29*, 177–185. [[CrossRef](#)] [[PubMed](#)]
33. Huang, E.P. Metal ions and synaptic transmission: Think zinc. *Proc. Natl. Acad. Sci. USA* **1997**, *94*, 13386–13387. [[CrossRef](#)] [[PubMed](#)]
34. Li, Y.; Hough, C.J.; Frederickson, C.J.; Sarvey, J.M. Induction of mossy fiber→CA3 long-term potentiation requires translocation of synaptically released Zn^{2+} . *J. Neurosci.* **2001**, *21*, 8015–8025. [[PubMed](#)]
35. Takeda, A. Insight into Glutamate Excitotoxicity from Synaptic Zinc Homeostasis. *Int. J. Alzheimers. Dis.* **2011**, *2011*, 491597. [[CrossRef](#)] [[PubMed](#)]



© 2017 by the authors. Licensee MDPI, Basel, Switzerland. This article is an open access article distributed under the terms and conditions of the Creative Commons Attribution (CC BY) license (<http://creativecommons.org/licenses/by/4.0/>).